Homogeneous nucleation rate measurements of 1-butanol in helium: A comparative study of a thermal diffusion cloud chamber and a laminar flow diffusion chamber

David Brus[a)]
Aerosol Laboratory, Institute of Chemical Process Fundamentals, Academy of Sciences of the Czech Republic, Rozvojová 135, 165 02 Prague 6, Czech Republic

Antti-Pekka Hyvärinen
Finnish Meteorological Institute, Sahaajankatu 20 E, 00880 Helsinki, Finland

Vladimír Ždímal
Aerosol Laboratory, Institute of Chemical Process Fundamentals, Academy of Sciences of the Czech Republic, Rozvojová 135, 165 02 Prague 6, Czech Republic

Heikki Lihavainen
Finnish Meteorological Institute, Sahaajankatu 20 E, 00880 Helsinki, Finland

(Received 14 January 2005; accepted 25 March 2005; published online 6 June 2005)

Isothermal homogeneous nucleation rates of 1-butanol were measured both in a thermal diffusion cloud chamber and in a laminar flow diffusion chamber built recently at the Institute of Chemical Process Fundamentals, Academy of Sciences of the Czech Republic, Prague, Czech Republic. The chosen system 1-butanol-helium can be studied reasonably well in both devices, in the overlapping range of temperatures. The results were compared with those found in the literature and those measured by Lihavainen in a laminar flow diffusion chamber of a similar design. The same isotherms measured with the thermal diffusion cloud chamber occur at highest saturation ratios of the three devices. Isotherms measured with the two laminar flow diffusion chambers are reasonably close together; the measurements by Lihavainen occur at lowest saturation ratios. The temperature dependences observed were similar in all three devices. The molecular content of critical clusters was calculated using the nucleation theorem and compared with the Kelvin equation. Both laminar flow diffusion chambers provided very similar sizes slightly above the Kelvin equation, whereas the thermal diffusion cloud chamber suggests critical cluster sizes significantly smaller. The results found elsewhere in the literature were in reasonable agreement with our results. © *2005 American Institute of Physics*. [DOI: 10.1063/1.1917746]

INTRODUCTION

Homogeneous nucleation is the initial step in the formation of liquid droplets from condensable vapors. Nucleation rate is rate of formation of critical clusters, the molecular clusters that have an equal probability to grow to a droplet or decay back to the vapor phase. If there is a need to measure homogeneous nucleation rates with a sufficient precision, the requirements for experimental methods adequately increase. According to Kashchiev[1] and Anisimov and Cherevko,[2] isothermal nucleation rates measured as functions of the saturation ratio yield the molecular content of critical clusters. Measuring isothermal nucleation rates has thus set the standard for nucleation rate measurements. Only a handful of devices are able to fulfill such requirements at the present time; these are the fast expansion cloud chamber,[3,4] two-piston expansion cloud chamber,[5,6] shock tube,[7,8] supersonic nozzles,[9] thermal diffusion cloud chamber[10–15] (TDCC), and laminar flow diffusion chamber[16–19] (LFDC). The experimental data show large scatter, which has been a point of discussion for a long time. For example, the measured nucleation rates of 1-pentanol can differ by several orders of magnitude depending on the measuring device. Attempts have been made to rule out reasons for the scatter in data, most notably the Joint Experiment on Homogeneous Nucleation initiated in Prague, June 1995.[20] However, comparison studies for understanding the experimental factors leading to different results are still lacking.

For this work, the homogeneous nucleation rates of 1-butanol were measured in parallel in a TDCC and in a LFDC built recently at the Prague Institute. The system 1-butanol-helium was chosen because it can be studied reasonably well with both devices in an overlapping temperature range. The new LFDC is based on a design of Lihavainen and Viisanen[21] and having the same experimental setup. The results of the TDCC, the new LFDC, and those of Lihavainen[22] were compared. A comparison with other measurements found in the literature was also made. The aim of the study is to gain a better understanding of experimental factors contributing to different results of measuring devices.

[a)]Electronic mail: brus@ipcf.cas.cz

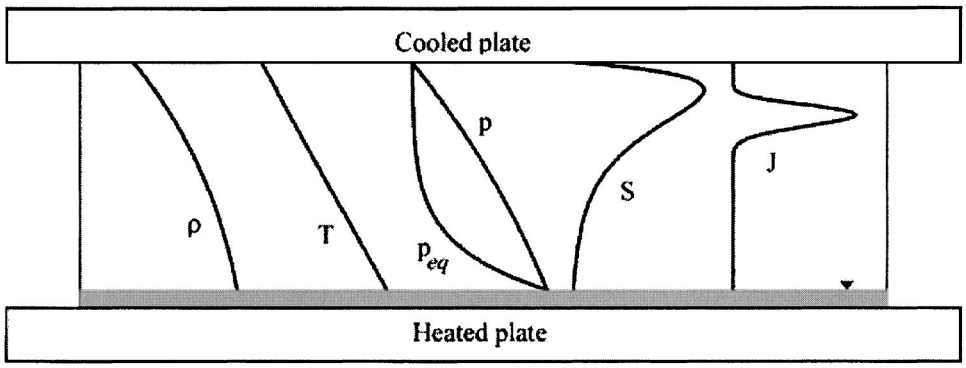

FIG. 1. Vertical 1D profiles of density, temperature, equilibrium and partial vapor pressures, saturation ratio, and nucleation rate inside TDCC.

II. EXPERIMENT, OPERATION PRINCIPLE, AND SETUP

A. The thermal diffusion cloud chamber

The used TDCC is presented in detail elsewhere.[23] A short overview of the technique is given here. The basic function of the diffusion cloud chamber is to produce supersaturated vapor by using nonisothermal diffusion. The chamber is designed so that one-dimensional diffusion of vapor takes place through an inert carrier gas. The chamber consists of two circular hard aluminum plates, separated by a 25-mm high ring made of a 5-mm-thick optical glass with an inner diameter of 160 mm. The bottom plate covered with a thin film (less than 1 mm) of the studied liquid is heated. The liquid evaporates from the film surface, diffuses through an inert gas, and condenses on the cooler top plate. The condensate flows along the glass wall back to the pool, so the chamber can be operated at a steady state. The type and pressure of the inert gas are chosen so that the density profile is stable to buoyancy-driven convection. Under such circumstances, the character of transport processes between the plates leads to a state, where both the temperature T and the partial vapor pressure p_A decrease almost linearly with increasing chamber height (see Fig. 1). Since the equilibrium vapor pressure p_{eq} decreases with the height more quickly than p_A, the vapor in the chamber becomes supersaturated with a maximum supersaturation $S=p_A/p_{\mathrm{eq}}$ reached close to the top plate.

By increasing the temperature difference between both plates, the supersaturation can be increased until it is sufficient for homogeneous nucleation to start. The self-cleaning nature of the chamber hinders heterogeneous nucleation. The nucleation induced by ions is effectively prevented by applying an electrostatic field across the chamber. Stable clusters of the new phase grow rapidly to visible droplets inside a thin layer called nucleation zone with nucleation rate maximum located somewhere below supersaturation maximum. The formed droplets fall back to the liquid film due to gravitation. The nucleation rate determination is described later in a separate section.

B. The laminar flow diffusion chamber

The laminar flow diffusion chamber (LFDC) is based on a method proposed by Anisimov *et al.*[24] The LFDC used in this investigation is based on a design of Lihavainen and Viisanen.[21] The operational principle of the LFDC is similar to the static diffusion cloud chamber. The LFDC consists of three main parts: a saturator, a preheater, and a condenser (Fig. 2). The carrier gas first enters a horizontal saturator containing the liquid under investigation. At the exit of saturator the carrier gas is saturated with the vapor. A laminar velocity profile is obtained in the preheater that is perpendicularly connected to the end of the saturator. The flowing vapor-gas mixture is then rapidly cooled in the condenser by heat exchange through the condenser wall. The temperature of the condenser is much lower than that of the saturator and hence high vapor supersaturation can be obtained due to a strong exponential dependence of equilibrium vapor pressure on temperature. In addition, an important principle of the LFDC operation is that the heat transfer by conduction is

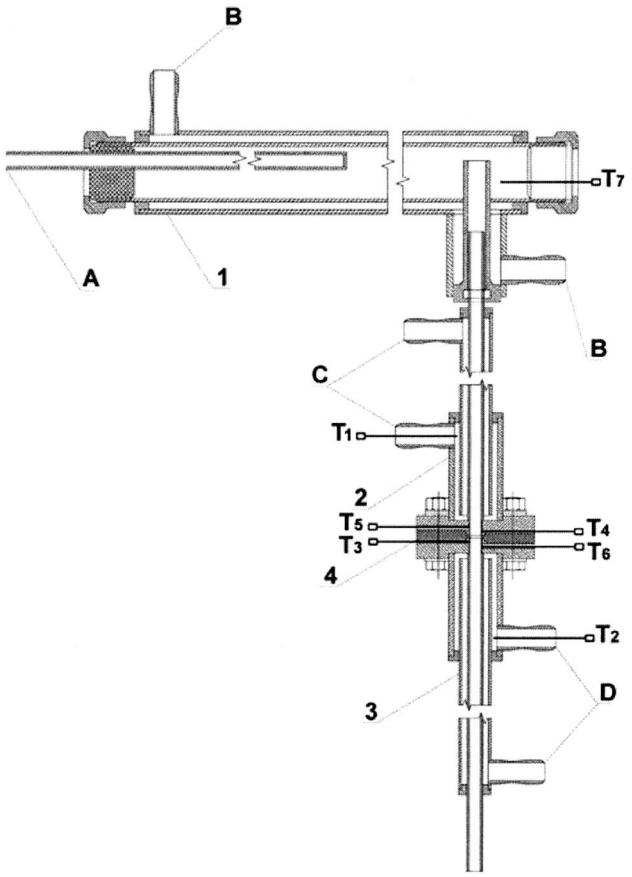

FIG. 2. Schematic picture of the LFDC. (1) saturator, (2) preheater, (3) condenser, (4) teflon spacer, (A) carrier gas inlet, (B) saturator thermostated liquid inlet and outlet, (C) preheater thermostated liquid inlet and outlet, and (D) condenser thermostated liquid inlet and outlet, T_1-T_7: thermocouples.

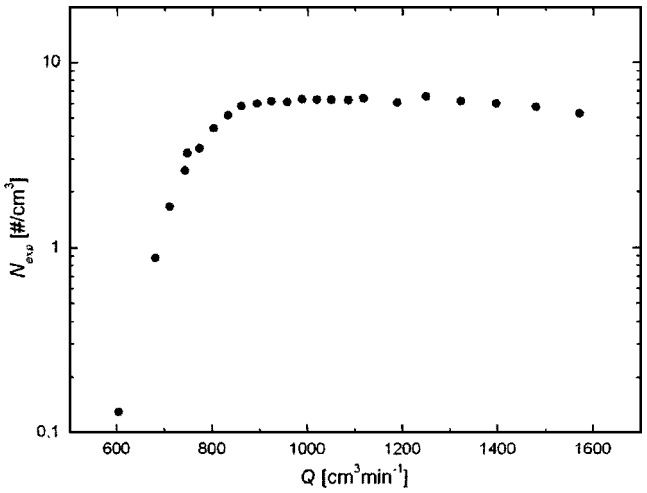

FIG. 3. The number of counted particles N_{exp} as a function of the flow rate Q in the LFDC (the flow rate test).

faster than the mass transfer by diffusion in the condenser tube. As a result, the equilibrium vapor pressure decreases faster than the partial pressure of the nucleating vapor which increases the saturation ratio. Also, a well-defined nucleation zone is produced in the axial region of the tube making data interpretation easier.

The ratio of the rates of heat transfer by conduction and mass transfer by diffusion is expressed by the Lewis number,

$$\mathrm{Le} = \frac{k}{D\rho c_p}, \tag{1}$$

where k is the thermal conductivity of the vapor-carrier gas mixture, D is the binary diffusion coefficient, ρ is the density of the mixture, and c_p is the specific heat of the mixture. For the correct operation of the LFDC, the Lewis number should be larger than unity. The Lewis number for 1-butanol in helium is 5.8.

Concentration of the vapor in the mixture is controlled by temperature of the saturator. To be sure of proper operation of the saturator in the LFDC, a flow rate test was made. The model predicts that at higher flow rates the nucleation rate is independent of the flow rate. At lower flow rates, with constant boundary conditions, the nucleation rate is lowered by several effects arising from the heat and mass transfer relations and also the vapor is considerably depleted already in the nucleation zone because of condensational growth of nucleated particles. Figure 3 illustrates how the number of counted particles rises to a certain value with increasing flow rate as these effects become negligible. When the flow rate is high enough the number of counted particles remains almost constant. However, if the flow rate becomes too high, the residence time in the saturator shortens so much that the carrier gas does not get fully saturated with the vapor any longer. The carrier gas flow rate of 1000 $\mathrm{cm}^3/\mathrm{min}$ was chosen for this investigation.

The level of supersaturation is controlled by the temperature difference between the saturator and the condenser. The nucleation temperature is controlled by temperatures of the preheater and the condenser. The flow is kept laminar to ensure that the transport processes are well defined. The number concentration of droplets is measured optically behind the condenser. A detailed description of the recently built LFDC is given below.

A schematic picture of the LFDC is presented in Fig. 2. The tubes connecting the carrier gas cylinder to the saturator are made of stainless steel designed for chromatography in order to avoid any contamination. The carrier gas flow was controlled by a mass flow controller (TESLA 306 KA/RA, Czech Republic) and checked with a soap bubble flow calibrator (Gilibrator 2, Sensidyne Inc., USA). After being filtered with a high efficiency particle absorber (HEPA), it is first introduced into the saturator. Inside the saturator, the carrier gas is brought into close contact and is fully saturated with the vapor of studied liquid.

The saturator is a 1-m-long tube with an inner diameter of 1.7 cm. The diameter of the saturator is smaller than in the design by Lihavainen and Viisanen.[21] This decreases the residence time of the carrier gas in the saturator but, on the other hand, the vapor diffusion distance from the liquid pool is shorter. The material of the saturator is stainless steel. The saturator is thermally insulated from the environment and its temperature is controlled with a thermostated circulating liquid bath (TB 150, VEB MLW, GDR). The end plugs of the saturator are made of Teflon. The tubing inlets for the carrier gas and the tubing inlets for the filling of studied liquid enter through a Teflon plug. The temperature of the saturator is measured with a chromel-alumel thermocouple (VEB Walzwerk Hettstedt), which is immersed in the liquid pool and situated near the inlet of the vapor-gas mixture into the preheater. The preheater inlet is situated above the liquid level inside the saturator.

The preheater is a 0.3-m and the condenser a 0.5-m-long tube, both with a 4.0 mm inner diameter. The inner tubes are made of stainless steel and the heating and cooling jackets are made of brass. The temperatures of the tubes are controlled by circulating liquid baths with thermostat (TB 150, VEB MLW, GDR) in the case of the preheater and with cryostat (MK70, VEB MLW, GDR) in the case of the condenser. The circulating liquid used for the parts of the LFDC was either water or ethanol depending on the required temperature. The temperatures of the preheater and the condenser are measured with chromel-alumel thermocouples (VEB Walzwerk Hettstedt, GDR) placed inside the circulation inlet of the preheater and outlet of the condenser, respectively, both situated about 4 cm from the Teflon spacer. Both the preheater and the condenser are thermally insulated from the environment. The preheater and the condenser are positioned vertically, therefore there are no settling losses of particles in the chamber. The vapor-gas mixture flows downward so that the liquid condensing on the wall of the condenser does not go back into the preheater and disturb the boundary conditions.

The temperature drop in the connecting piece between the preheater and the condenser has to be as steep as possible. This is reached by separating the preheater and condenser tubes with Teflon spacer. Because the heat conductivity of stainless steel is about 100 times higher than that of Teflon, it is assumed that the temperatures of the preheater

and the condenser are independent. Holes for measuring the temperature gradient are drilled in the brass jacket and in both sides of the Teflon spacer (see Fig. 2).

The Teflon spacer is 1.2 mm thick at the shoulders and 4.6 mm elsewhere. The inner surface of the tubes at the connection between the preheater and the condenser is smooth in order not to affect the flow profile inside.

The liquid condensed on the walls of the condenser is subsequently separated from the gas flow with a specially designed collector made of brass and attached to the end of the condenser. Unlike the design by Lihavainen, where the aerosol had to take a 90° turn, here the aerosol flow continues straight on. There is a slight widening at the upper part of the collector which allows the condensate to flow to a closed reservoir. The reservoir has a small drilled outlet which facilitates its emptying. The collector is thermally insulated from the environment. To avoid evaporation of droplets, the collector is cooled with ice if low-temperature isotherms are measured.

The gas-vapor mixture including the formed particles then continues to the optical cell where the particles are counted. The optical cell is a 9-cm-long glass ring with a 5.4-cm inner diameter. The counting system consists of a small diode laser including a beam shaping lens, a photomultiplier tube, and electronics for discrimination and counting (courtesy of the Department of Physical Chemistry, Philipps-Universität Marburg, Germany). The counting system is different from that of Lihavainen, who used an optical head of a CPC 3010 for counting of particles.

All measurements were made at atmospheric pressure. It is expected that this is also the pressure inside the LFDC.

The temperature-measuring systems used both in the recently built LFDC and in the TDCC were calibrated against a Hewlett–Packard quartz digital thermometer (whose accuracy is kept within 0.01 K of the temperatures on the ITS-90 by regularly calibrated against a platinum resistance thermometer Leeds&Northrup provided with National Bureau of Standard certificate). The resulting uncertainty in determination of temperature in the recently built LFDC does not exceed 0.1 K. The uncertainty for TDCC is constant over a long period of time (several years) and it does not exceed 0.05 K even at the boundaries of the temperature range used. The precision of temperature measurement in experiments of Lihavainen[22] was 0.05 K.

III. DATA EVALUATION

A. The TDCC

The new data evaluation method of TDCC has not been described yet, so it will be given in more detail here, including the description of the photographic method, subsequent image analysis, and determination of the experimental nucleation rate.

1. Photographic method

The photographic method itself was already described in detail by Smolík and Ždímal.[25] The optical system at present consists of a He–Ne laser, beam shaping optics, and a charge-coupled device (CCD) camera. The flattened laser beam illuminates the whole height of the chamber from a side, passing through its axis. Trajectories of droplets, formed inside this beam, can be recorded by a CCD camera positioned exactly perpendicularly to the beam (Fig. 4).

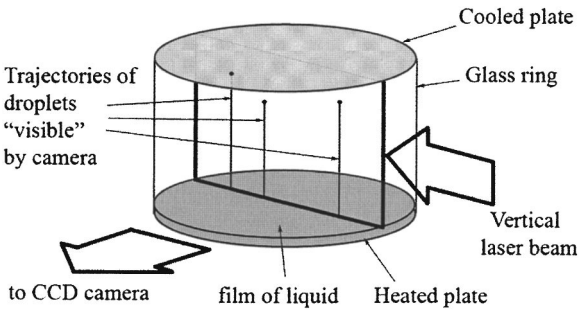

FIG. 4. Scheme of the photographic method.

The CCD camera used in this work is a 16-bit camera ST-7 XME (SBIG Instrument Group, USA) widely used in astronomy for imaging of faint objects. It was chosen for its sensitivity and acceptable resolution (756×512 pixels). A standard objective Micro-Nikkor of a 55-mm focal length was connected to the camera via adapter. The camera is controlled by a software, which enables taking series of pictures with predetermined parameters. The noise caused by camera electronics (the CCD microchip working temperature is $-5\ ^\circ\mathrm{C}$) is usually negligible in comparison with optical noise and reflections from the experiment. This results in quality of the pictures comparable with that of photographs made by classical analog camera used in previous experiments, e.g., Ždímal and Smolík.[23] The typical picture taken by a CCD camera can be seen in Fig. 5.

2. Image analysis

The obtained digital images are evaluated automatically using image analysis (Ždímal *et al.*)[26]

Each droplet photographed can be characterized by its starting point (point of its origin) and its trajectory ending in the liquid pool at the bottom plate. The starting points of droplet trajectories are detected as local maxima of normal-

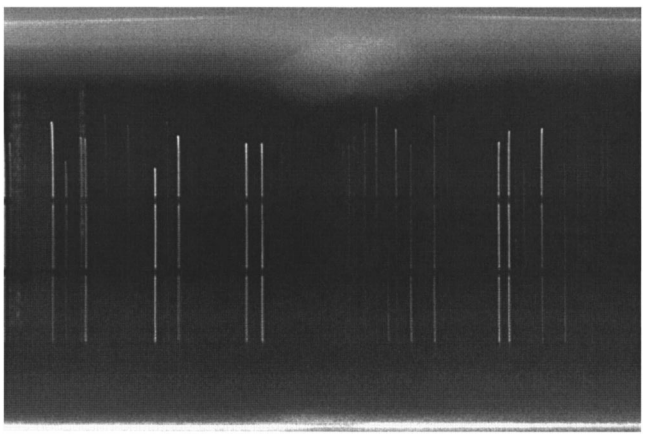

FIG. 5. The typical image downloaded from CCD camera, the white horizontal lines at the bottom and at the top represent liquid films on the bottom and on the top plates of the chamber; the white vertical lines denote droplets' trajectories.

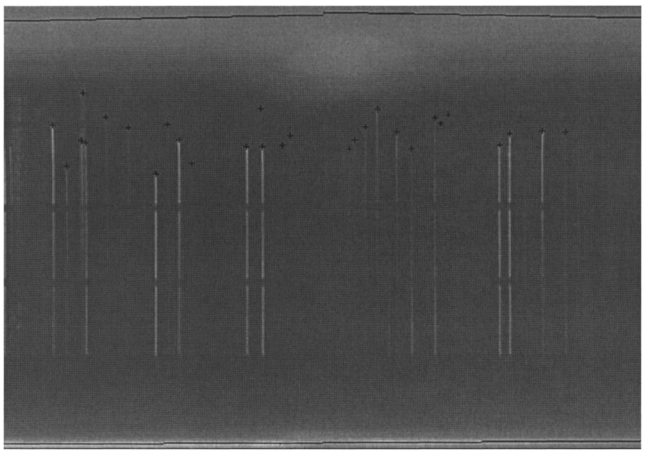

FIG. 6. The CCD image after processing by image analysis, the black horizontal lines at the bottom and the top represent found positions of liquid films. The white vertical lines denote droplets' trajectories and the black crosses mean assigned positions of starting points.

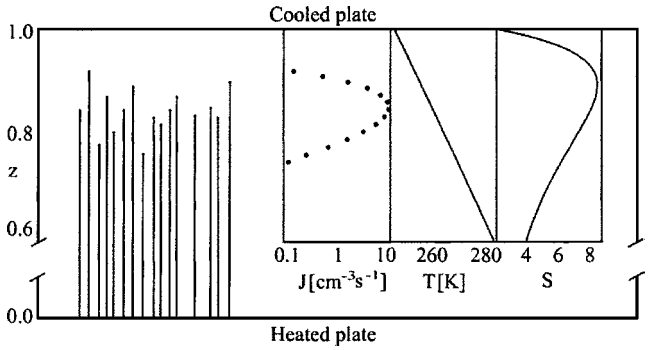

FIG. 7. The method of TDCC data evaluation that relates experimental values of homogeneous nucleation rate to corresponding previously calculated values of temperature and supersaturation.

ized correlation with a user-defined template. High values of normalized correlation are obtained also in the close neighborhood of the found droplet, therefore the algorithm of suppression of nonmaximum response signal is implemented. The width of the surroundings, in which only the pixel with maximal intensity is accepted as a droplet starting point, is an optional parameter of the program. The suppression of nonmaximal values has several consequences, e.g., it defines minimal distance between two detected droplets. This can strongly affect the distribution histogram of the found droplets, because only one of two droplets can be detected in the surroundings for suppression. This behavior is more probable at high densities of droplets, e.g., at higher nucleation rates or long exposure times. The suppression of response signal in the same column was also implemented; hence it is impossible to find another droplet at a lower position than the already found droplet. The aim of the latter algorithm is to remove false signals that can appear on the trajectories of formed droplets, since the trajectories are interrupted several times by a shadow of heating wires.

The position of liquid films defines the coordinate system and is found by a randomized optimization approach. The criterion function, the sum of intensities along the line, is evaluated from a set of samples; typically it is 10% of pixels along a line. An exhaustive search is performed in the space of nearly horizontal line at the bottom liquid film and a pair of lines is searched in the case of conical ceiling. The overall processing is completed within few seconds on a standard Pentium personal computer (PC).

A typical CCD image after processing can be seen in Fig. 6. The black horizontal lines at the bottom and the top express the found positions of liquid films. The white vertical lines denote trajectories of droplets and the black crosses mean assigned positions of starting points. The estimated error in determining vertical position is less than 1 pixel. The capability of processing series of pictures automatically makes this method very effective.

After evaluating sufficient number of droplets (starting points) in one experiment, one gets the number distribution of droplets as function of the chamber height. Subsequent division of the number distribution by a photographed volume and exposure time gives the homogeneous nucleation rate (drops per cm^3/s) as a function of height in the chamber. The homogenous nucleation rate distribution is subsequently fitted by Gaussian distribution. This method gives $J_{exp}(z)dz$, the experimentally determined homogeneous nucleation rate, as a function of vertical position inside the chamber, z. The local values of the nucleation rate are related to the corresponding values of temperature and supersaturation calculated using a one-dimensional (1D)model of mass and heat transport in the TDCC[10,27] (see Fig. 7), and the resulting dependence $J_{exp}(T,S)$ can be directly compared with theoretical predictions of any nucleation theory.

B. The LFDC

The data evaluation method has been reported elsewhere in detail,[21] and only a short overview is given here.

The profiles of the temperature, partial vapor pressure, and equilibrium vapor pressure in the condenser have to be known before the nucleation rates can be calculated from the measured particle concentrations. The profiles cannot be measured without disturbing the flow, but they can be calculated by solving the equations for heat and mass transfer, equations of motion, and the equation of continuity for the laminar flow. These differential equations are solved numerically under certain assumptions[22] with the following boundary conditions:

$$T(r, z = z_0) = T_{pr}, \tag{2a}$$

$$T(R_0, z_0 < z \leqslant 0) = T_{pr}, \tag{2b}$$

$$T(R_0, z > 0) = T_{cond}, \tag{2c}$$

$$\omega(r, z = z_0) = \omega_{eq}(T_s), \tag{3a}$$

$$\omega(R_0, z_0 < z \leqslant 0) = \omega_{eq}(T_s), \tag{3b}$$

$$\omega(R_0, z > 0) = \omega_{eq}(T_{cond}). \tag{3c}$$

In Eqs. (2) and (3), T_{pr}, T_{cond}, and T_s are the temperatures of the preheater, condenser, and saturator, respectively, $\omega_{eq}(T_i)$ is the mass fraction of the nucleating vapor defined by equilibrium vapor pressure at the temperature T_i, $z=0$ is the

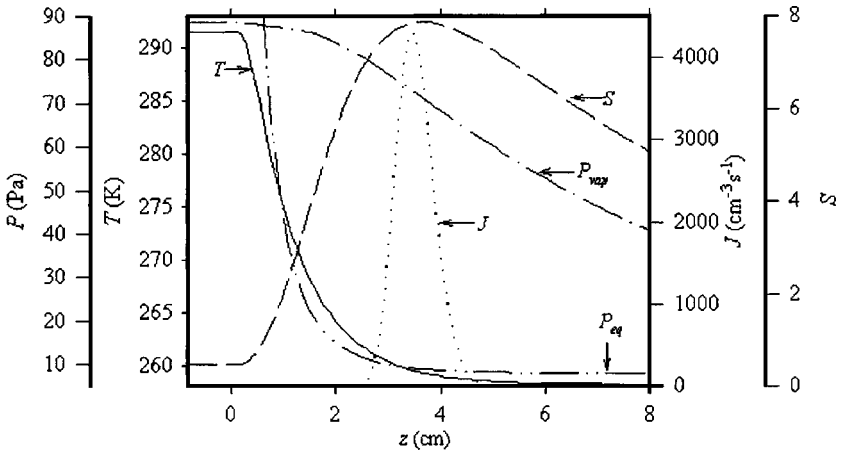

FIG. 8. An example of calculated profiles, at the axis of LFDC tube, of temperature (Ref. 22) T, equilibrium vapor pressure p_{eq} and vapor pressure p_{vap}, saturation ratio S, and nucleation rate J, as a function of axial position in the condenser.

boundary between the preheater and the condenser, and z_0 is the starting position of the calculations in the preheater.

The new construction of the LFDC enabled measuring the temperature near and around the $z=0$ position, i.e., in the neighborhood of the Teflon spacer. In a typical measurement, the temperature difference between the preheater and the condenser, T_1 and T_2 in Fig. 2 is about 30 K. The temperature difference between T_1 and T_5 in Fig. 2 was about 0.15 K, and between T_2 and T_6 in Fig. 2 about 2.5 K. The boundary conditions in the model were changed accordingly to see the effect on the nucleation rates. The difference of the results was less than 0.1% in the saturation ratio and less than 0.6% in the experimental nucleation rate. Thus, it was concluded that Eqs. (2) and (3) express boundary conditions, and it is adequate to measure the temperatures of the preheater and the condenser from the circulation liquid.

An example of the calculated profiles of temperature, vapor pressure, equilibrium vapor pressure, saturation ratio, and theoretical nucleation rate are presented in Fig. 8. Nucleation occurs in a narrow region at the axis of the tube. Both the saturation ratio and the temperature are well defined in this region where the theoretical nucleation rate reachesits maximum value. The corresponding experimental maximum nucleation rate $J_{\mathrm{exp}}^{\mathrm{max}}$ can be obtained using the relationship proposed by Wagner and Anisimov.[28]

$$\frac{J_{\mathrm{exp}}^{\mathrm{max}}}{\int J_{\mathrm{exp}} dV} = \frac{J_{\mathrm{the}}^{\mathrm{max}}}{\int J_{\mathrm{the}} dV}. \tag{4}$$

In Eq. (4), $J_{\mathrm{the}}^{\mathrm{max}}$ is the theoretical nucleation rate maximum, $\int J_{\mathrm{the}} dV$ is the theoretical nucleation rate integrated over the volume of the condenser, and $\int J_{\mathrm{exp}} dV$ is the measured particle flow multiplied by the flow rate. The choice of nucleation theory does not affect the value of $J_{\mathrm{exp}}^{\mathrm{max}}$ considerably.[17,29] The classical nucleation theory (CNT)[30] was used to predict nucleation rates. The nucleation rate J in the CNT is expressed as

$$J_{\mathrm{CNT}} = \upsilon N^2 \sqrt{\frac{2\sigma}{\pi m}} \exp\left[-\frac{16\pi\sigma^3\upsilon^2}{3(kT)^3(\ln S)^2} \right], \tag{5}$$

where N is the number concentration of molecules, υ is the molecular volume, σ is the surface tension, m is the mass of a molecule, T is the temperature, S is the saturation ratio, and k is the Boltzmann constant.

The thermodynamic parameters of 1-butanol and helium which are needed to solve the transport equations are the same for both the TDCC and the LFDC and are presented in Table I. The parameters are the same as used by Lihavainen.[22] The temperature ranges used in both devices for each isotherm are very similar. Moreover, the temperature range in which the transport parameters vary in the LFDC is only slightly narrower than the corresponding temperature range in the TDCC. Therefore, it is expected that even if the relationships used for calculation of individual transport parameters were not the optimal ones, this would not change the relative position of the resulting isotherms.

IV. RESULTS AND DISCUSSION

Homogeneous nucleation rates ranging from about 10^{-1} to 10^2 cm^{-3} s^{-1} using the TDCC and from about 10^2 to 10^5 cm^{-3} s^{-1} using the LFDC were measured for 1-butanol. Helium (Linde, purity 99.996%) was used as a carrier gas. The lower limit for the TDCC is due to difficulties in running very long experiments (many hours) and the higher limit to vapor depletion and a latent heat release effect. The lower limit of the rates measured with the LFDC is mostly due to the ion-induced nucleation, the higher limit is due to the efficiency of the counting system. The nucleation temperatures used in TDCC were from 265 to 290 K and for LFDC from 265 to 280 K. The isotherms were chosen with a step of 5 K (265, 270, 275, 280, and 290 K for TDCC only), in the range that could be easily managed by experimental setup used in this work. The low-temperature limit for the LFDC in this work was defined by evaporation of droplets before counting. The high temperature is limited by depletion of vapor and heat released by condensation. All the LFDC measurements were made at atmospheric pressure. To avoid any convection inside the TDCC, the total pressure must remain below a limiting value that depends on the temperature, condensable vapor, and background gas.[31,32] The pressure in the TDCC was varied from 11 kPa at $T_n=265$ K to 120 kPa at $T_n=290$ K. To test whether the carrier gas pressure has an influence on the results, the isotherm $T_n=290$ K was also measured at 50 kPa.

TABLE I. Thermodynamic properties. Subscript v=vapor, subscript g=gas, subscript vg=vapor-gas mixture, M=molar mass, T_b=boiling temperature, T_c=critical temperature, P_c=critical pressure, V_c=critical volume, Ω=Pitzer acentric factor, μ=dipole moment, ΔH=enthalpy of vaporization, p_{eq}=equilibrium vapor pressure, γ=surface tension, c_p=heat capacity, λ=thermal conductivity, D=diffusion coefficient, η=viscosity, α=thermal diffusion factor, and ρ=density.

Property	*n*-butanol	Unit	Ref.
M	74.123	kg kmol^{-1}	
T_b	390.88	K	
T_c	563.05	K	Poling (Ref. 36)
P_c	4.423×10^{6}	Pa	Poling (Ref. 36)
V_c	2.75×10^{-1}	m^3 kmol^{-1}	
Ω	0.590	l	Poling (Ref. 36)
M	1.8	Debye	Poling (Ref. 36)
σ_v	5.645×10^{-10}	m	
ε_v/k	593.06	K	
$c_{p,v}$	$3266+4.18\times10^{2}T-2.242\times10^{-1}T^2+4.685\times10^{-5}T^3$	J kmol^{-1} K^{-1}	Reid (Ref. 37)
λ_v	$-7.772\times10^{-3}+3.564\times10^{5}T+1.206\times10^{-7}T^2-4.992\times10^{-11}T^3$	W m^{-1} K^{-1}	Yaws (Ref. 38)
λ_l	$2.288\times10^{-1}-2.697\times10^{-4}T-1.323\times10^{-8}T^2$	W m^{-1} K^{-1}	Reid (Ref. 37)
η_v	$10^{-7}(-18.43+0.2867\times T-10.48^{-6}\times T^2)$	Pa s	Yaws (Ref. 38)
ρ_l	$824.6-0.75(T-273.15)$	kg m^{-3}	Strey and Schmeling (Ref. 39)
γ_1	$10^{3}[25.98-0.08181(T-273.15)]$	N m^{-1}	Strey and Schmeling (Ref. 39)
P_v^{eq}	$\exp(98.494-9412.6064/T-10.54\times\log T)$	Pa	Schmeling and Strey (Ref. 40)
ΔH_v	$43.095\times10^{6}[(T_c-T)/(T_c-T_b)]^{0.38}$	J kmol^{-1}	Yaws (Ref. 38)

Property	helium	Unit	Ref.
M	4.0026	kg kmol^{-1}	
σ_g	2.551×10^{-10}	m	
ε_g/k	10.22	K	
c_p	5200	J kg^{-1} K^{-1}	Reid (Ref. 37)
λ_g	$(-5.8543\times10^{-5}+2.68606\times10^{-6}\times T-7.00113\times10^{-9}\times T^2+1.07396\times10^{-11}\times T^3-6.01768\times10^{-15}\times T^4)4.1868\times100$	W m^{-1} K^{-1}	Hung *et al.* (Ref. 41)
η_g	$1.4083.10^{-6}T^{1.5}/(T+70.22)$	Pa s	Hung *et al.* (Ref. 41)

Property	*n*-butanol in helium	Unit	Ref.
D_{vg}	$10^{-4}(0.00143\times T^{1.75}/[(P/100000)7.5951^{0.5}(92.81^{1/3}+2.67^{1/3})^2]$	m^2 s^{-1}	Fuller[a]
$1/\alpha$	$[-0.62264+T/(-23.4305+0.30537\times T)](y+0.1548)+0.0964$		Vašáková and Smolík (Ref. 42)
λ_{vg}	$x_v\lambda_v/(x_v+A_{vg}x_g)+x_g\lambda_g/(x_g+A_{gv}x_v)$	W m^{-1} K^{-1}	Reid (Ref. 37)
σ_{vg}	4.098×10^{-10}	m	
ε_{vg}/k	77.85	K	

[a]Method described in Reid *et al.*

A. Experimental nucleation rates

The experimental and calculated data for the nucleation rates obtained using the TDCC are presented in Table II, and data from new LFDC in Table III. The nucleation rates as a function of the saturation ratio are presented in Fig. 9. Also the measurements by Lihavainen are shown. The same isotherms measured with the TDCC occur at the highest saturation ratios of the three devices. Isotherms measured with the two LFDCs are reasonably close together, the measurements by Lihavainen occur at lowest saturation ratios. It is interesting to note that the isotherms measured using the TDCC fall almost on the same line, but 10 K lower, than the isotherms measured by Lihavainen throughout the temperature range. This raises the question whether the temperature measurements can explain the differences in the results. To make the Lihavainen 265-K isotherm correspond with the TDCC data, the temperature measurement of the saturator would have to fail about 3.0 K. This is highly unlikely. Likewise, the temperatures in the TDCC would have to fail about 0.7 K concerning both plates, lowering temperature of the lower plate and increasing temperature of the upper plate.

The slopes of the isotherms are different depending on the measuring device. The isotherms measured by using the new LFDC have the steepest slopes, while the ones measured by using the TDCC are the flattest.

Due to the stability issues mentioned above the isotherms in the TDCC had to be studied at different total pressures. Knowing that pressure of the carrier gas may have a slight effect on the observed nucleation rate in the TDCC, the 290-K isotherm has been studied at 50 and 120 kPa. The obtained isotherms do not seem to be separated from each other. This indicates that the influence of helium pressure in a given pressure range on the observed nucleation rate can be probably neglected.

The dotted error lines in Fig. 10 are estimated from the inaccuracies of temperature measurements in the TDCC and the LFDC. The temperature error estimation concerning TDCC is calculated by assuming that the most significant

TABLE II. The nucleation rate of 1-butanol in helium, measured with the TDDC.

T_b, K	T_t, K	T_n, K	p_{tot}, kPa	S_n	J_{exp}, cm^{-3} s^{-1}
T=265 K, p=12 kPa					
300.85	252.84	265	11.4	5.90	4.11*E*1
300.67	252.85	265	11.4	5.84	2.61*E*1
302.16	254.08	265	11.5	5.95	1.00*E*2
301.88	254.18	265	11.5	5.82	4.08*E*1
301.60	254.22	265	11.5	5.72	1.18*E*1
301.28	254.20	265	11.5	5.63	4.88*E*0
300.99	254.24	265	11.5	5.52	4.40*E*-1
301.39	254.14	265	11.6	5.67	9.18*E*0
301.29	254.15	265	11.6	5.63	4.20*E*0
301.14	254.20	265	11.6	5.57	1.30*E*0
300.94	254.22	265	11.6	5.50	1.18*E*0
301.21	254.16	265	11.6	5.61	5.81*E*0
T=270 K, p=15 kPa					
T_b, K	T_t, K	T_n, K	p_{tot}, kPa	S_n	J_{exp}, cm^{-3} s^{-1}
307.14	258.47	270	14.9	5.48	1.31*E*2
306.87	258.52	270	14.9	5.39	7.27*E*1
306.61	258.59	270	14.9	5.30	2.81*E*1
306.32	258.6	270	14.9	5.21	1.37*E*1
306.05	258.70	270	14.9	5.11	5.05*E*0
305.75	258.72	270	15.8	4.99	8.63*E*-1
305.03	258.72	270	15.8	4.80	2.03*E*-1
T=275 K, p=30 kPa					
T_b, K	T_t, K	T_n, K	p_{tot}, kPa	S_n	J_{exp}, cm^{-3} s^{-1}
313.97	264.78	275	29.1	4.77	7.60*E*1
313.56	264.8	275	29.1	4.67	2.86*E*1
313.45	264.93	275	29.1	4.61	1.01*E*1
313.27	264.98	275	29.0	4.56	5.69*E*0
313.17	264.91	275	29.4	4.55	9.64*E*0
313.15	264.99	275	29.4	4.52	3.71*E*0
312.93	265.01	275	29.4	4.47	3.30*E*0
313.06	265.08	275	29.3	4.48	2.77*E*0
313.05	265.24	275	29.3	4.43	1.74*E*0
312.91	265.34	275	29.3	4.37	1.16*E*0
313.08	263.76	275	30.3	4.82	7.22*E*1
312.82	263.83	275	30.4	4.74	4.88*E*1
312.54	263.90	275	30.3	4.66	1.53*E*1
312.25	263.96	275	30.3	4.58	6.10*E*0
311.98	264.03	275	30.3	4.50	8.89*E*-1
T=280 K, p=30 kPa					
T_b, K	T_t, K	T_n, K	p_{tot}, kPa	S_n	J_{exp}, cm^{-3} s^{-1}
315.80	267.82	280	30.0	4.21	4.31*E*0
315.78	268.07	280	30.0	4.16	2.74*E*0
315.57	268.32	280	29.3	4.08	6.29*E*-1
317.20	268.32	280	30.2	4.39	4.01*E*1
317.15	268.44	280	30.2	4.35	2.54*E*1
316.93	268.48	280	30.2	4.30	1.38*E*1
316.72	268.51	280	30.2	4.25	8.73*E*0
316.37	268.16	280	30.4	4.25	7.39*E*0
316.26	268.24	280	30.4	4.21	4.93*E*0
315.74	268.21	280	30.3	4.12	3.08*E*0
317.62	268.41	280	31.0	4.44	7.98*E*1
317.36	268.47	280	31.0	4.38	2.99*E*1
317.07	268.53	280	31.0	4.30	9.38*E*0
316.80	268.60	280	31.0	4.23	8.94*E*0

TABLE II. (*Continued.*)

T_b, K	T_t, K	T_n, K	p_{tot}, kPa	S_n	J_{exp}, cm^{-3} s^{-1}
T=265 K, p=12 kPa					
316.55	268.48	280	31.0	4.21	3.03*E*0
T=290 K, p=50 kPa					
323.66	275.27	290	46.9	3.56	1.49*E*0
323.51	275.32	290	46.9	3.53	1.00*E*0
323.18	275.37	290	46.8	3.48	2.76*E*−1
327.82	278.22	290	48.4	3.76	4.30*E*1
327.54	278.29	290	48.4	3.70	1.15*E*1
327.27	278.37	290	48.3	3.65	4.97*E*0
327.02	278.44	290	48.2	3.60	3.69*E*0
328.08	278.21	290	48.5	3.80	6.87*E*1
328.12	278.17	290	48.4	3.82	6.40*E*1
T=290 K, p=120 kPa					
326.30	274.25	290	120.1	3.82	6.43*E*1
326.19	274.39	290	119.9	3.79	4.33*E*1
325.80	274.42	290	119.8	3.73	1.78*E*1
325.71	274.46	290	119.7	3.71	8.57*E*0
325.39	274.55	290	119.7	3.65	4.05*E*0
325.35	274.65	290	119.6	3.63	3.16*E*0
325.46	274.63	290	118.7	3.65	3.39*E*0
325.33	274.67	290	118.6	3.63	3.24*E*0
325.11	274.71	290	118.5	3.59	2.17*E*0
325.02	274.75	290	117.8	3.57	1.37*E*0
327.52	275.33	290	119.6	3.86	8.33*E*1
328.50	276.39	290	120.1	3.85	4.17*E*1
329.24	277.60	290	120.5	3.76	2.02*E*1
328.97	277.65	290	120.4	3.71	8.69*E*0
328.67	277.73	290	120.2	3.65	2.56*E*0

error can be made in determining the position of liquid films on the lower and upper plates. This can be done by changing the saturation ratio of the lower-most and the upper-most experimental nucleation rate points on one isotherm by increasing or decreasing the distance between liquid films (1 pixel in both directions for both films). Only the lower-most and the upper-most experimental nucleation rate points which lie on or very close to the linear fit for all experimental points of each isotherm were taken into consideration; hence several points can be found outside the region determined by the dotted error lines. In this way, it is possible to obtain the space in which both the position and the slope of the isotherm can alternate.

In the LFDC this is done by changing the temperatures of the saturator, preheater and condenser by the estimated error of the thermocouples (0.1 K) at the maximum or minimum saturation ratio. The experimental nucleation rates are calculated with the new boundary conditions. The dotted error lines edges in Fig. 10 represent the results calculated in this way. It should be noted that changing the temperatures in the LFDC calculations changes also the nucleation temperature.

B. Critical cluster sizes

The critical cluster sizes can be calculated from the slopes of the nucleation rate isotherms according to the nucleation theorem:[1,2]

$$\left(\frac{\partial \ln J}{\partial \ln S}\right)_T \approx n^*. \tag{6}$$

In Eq. (6) n^* is the number of molecules in the critical cluster. The theoretical radius of the critical cluster r^* can be obtained from the Kelvin equation,

$$r^* = \frac{2\sigma v_{liq}}{kT \ln S}, \tag{7}$$

where v_{liq} is the volume of a liquid molecule and S is the experimental critical saturation ratio. Looking at the Kelvin equation, one sees that the critical cluster size depends both on the temperature and the saturation ratio. The number of molecules in the critical clusters is presented as a function of critical saturation ratio in Fig. 11. The critical saturation ratio is taken in the middle of each isotherm.

The measurements made in the new LFDC give the highest number of molecules in critical clusters. The mea-

TABLE III. The nucleation rate of 1-butanol in helium, measured with the LFDC. p is the total pressure, Q is the volumetric flow rate, T_{pr} is the temperature of the preheater, T_{cond} is the temperature of the condenser, T_{lab} is the temperature of the lab, T_s is the temperature of the saturator, T_n is the nucleation temperature, T_b is temperature of the bottom plate, T_t is temperature of the top plate, p_{tot} is total pressure, N is the particle concentration, S_n is the saturation ratio at the nucleation rate maximum, and J_{exp} is the experimental nucleation rate maximum.

p_{tot}, kPa	Q, $cm^3\ s^{-1}$	T_{pr}, K	T_{cond}, K	T_{lab}, K
101.3	16.81	296.85	263.06	298.15
T_s, K	T_n, K	N, cm^{-3}	S_n	J_{exp}, $cm^{-3}\ s^{-1}$
288.29	264.99	0.345	5.73	3.47*E*3
288.54	265.00	2.768	5.83	2.68*E*4
288.79	265.01	7.234	5.94	6.75*E*4
288.92	265.01	10.727	5.99	9.83*E*4
288.54	265.00	3.475	5.84	3.36*E*4
288.45	265.00	1.506	5.80	1.48*E*4
288.32	264.99	0.343	5.74	3.44*E*3
287.97	264.94	0.054	5.61	5.68*E*2
287.75	264.92	0.011	5.53	1.23*E*2
p_{tot}, kPa	Q, $cm^3\ s^{-1}$	T_{pr}, K	T_{cond}, K	T_{lab}, K
101.3	16.75	296.85	263.07	298.15
T_s, K	T_n, K	N, cm^{-3}	S_n	J_{exp}, $cm^{-3}\ s^{-1}$
287.78	264.96	0.038	5.53	4.14*E*2
287.98	264.97	0.076	5.61	8.07*E*2
288.23	264.98	0.402	5.70	4.09*E*3
288.50	264.99	1.617	5.81	1.58*E*4
288.84	265.00	7.768	5.96	7.21*E*4
p_{tot}, kPa	Q, $cm^3\ s^{-1}$	T_{pr}, K	T_{cond}, K	T_{lab}, K
101.3	16.72	301.41	268.01	298.15
T_s, K	T_n, K	N, cm^{-3}	S_n	J_{exp}, $cm^{-3}\ s^{-1}$
293.64	270.03	6.791	5.32	7.13*E*4
293.82	270.04	11.545	5.39	1.18*E*5
293.30	270.04	5.042	5.20	5.58*E*4
293.05	270.03	0.993	5.12	1.14*E*4
292.83	270.01	0.098	5.04	1.16*E*3
292.81	270.01	0.305	5.04	3.63*E*3
292.60	269.99	0.070	4.97	8.59*E*2
292.41	269.98	0.018	4.91	2.29*E*2
292.26	269.97	0.005	4.86	6.70*E*1
292.04	269.96	0.004	4.79	5.08*E*1
p_{tot}, kPa	Q, $cm^3\ s^{-1}$	T_{pr}, K	T_{cond}, K	T_{lab}, K
101.3	16.75	305.79	272.92	298.15
T_s, K	T_n, K	N, cm^{-3}	S_n	J_{exp}, $cm^{-3}\ s^{-1}$
297.58	275.09	0.286	4.52	3.90*E*3
297.37	275.07	0.097	4.46	1.35*E*3
297.19	275.06	0.050	4.41	7.14*E*2
297.06	275.06	0.009	4.37	1.29*E*2
296.91	275.05	0.010	4.33	1.56*E*2
297.55	275.08	0.141	4.51	1.93*E*3
297.97	275.11	3.078	4.62	3.96*E*4
298.16	275.12	4.117	4.68	5.14*E*4
298.33	275.13	10.805	4.73	1.32*E*5
297.76	275.10	1.104	4.57	1.46*E*4
297.60	275.09	0.396	4.52	5.37*E*3
297.44	275.08	0.235	4.48	3.26*E*3
p_{tot}, kPa	Q, $cm^3\ s^{-1}$	T_{pr}, K	T_{cond}, K	T_{lab}, K
101.3	16.67	310.64	277.65	298.15
T_s, K	T_n, K	N, cm^{-3}	S_n	J_{exp}, $cm^{-3}\ s^{-1}$
301.78	279.92	0.009	3.96	1.44*E*2

TABLE III. (*Continued.*)

p_{tot}, kPa	Q, $cm^3\ s^{-1}$	T_{pr}, K	T_{cond}, K	T_{lab}, K
101.3	16.81	296.85	263.06	298.15
T_s, K	T_n, K	N, cm^{-3}	S_n	J_{exp}, $cm^{-3}\ s^{-1}$
302.00	279.95	0.027	4.01	4.32*E*2
302.19	279.96	0.075	4.05	1.18*E*3
302.38	279.99	0.214	4.10	3.28*E*3
302.58	280.01	0.621	4.14	9.28*E*3
302.83	280.03	1.953	4.20	2.82*E*4
302.87	280.03	3.983	4.21	5.71*E*4
303.07	280.05	9.221	4.27	1.28*E*5
303.18	280.06	12.22	4.28	1.68*E*5

surements made in the TDCC give the lowest number of molecules in critical clusters. All the measurements give a similar trend for the critical cluster sizes, the critical cluster becomes smaller as the saturation ratio increases (or the temperature decreases). The exceptions to this trend are the 270- and 265-K isotherms measured in the TDCC and 265 K in the new LFDC. For the new LFDC this difference can be explained by evaporation of nucleated droplets before detection. The 270- and 265-K isotherms are close to the lower-temperature limit of the TDCC. For these isotherms the upper plate working temperature is 258 and 254 K, respectively. The humidity in the room air condenses on the upper plate heat exchanger (even when using blowing dry nitrogen to suppress condensation) causing a slight instability in the temperature measurement and subsequent error in experimental nucleation rate determination.

The molecular content error of the critical clusters was estimated both as a statistical error of the isothermal plots, the standard deviation (SD) included in Table IV, and as an error estimated from previously mentioned possible inaccuracies of the temperature measurements in the TDCC and LFDC. In order to estimate the uncertainties arising from inaccuracies of temperature measurements, the slope was calculated from the opposite corners of the dotted error lines presented in Fig. 10. In this way, two extreme values of the critical cluster size for each particular isotherm were obtained. This is illustrated in Fig. 11.

The difference between the calculated molecular contents of critical clusters and those predicted by the Kelvin equation are shown in Table IV. The Kelvin equation underestimates the critical cluster sizes obtained from both of the LFDCs, but overestimates the critical cluster sizes obtained from the TDCC.

C. Comparison with theory

The measured nucleation rates were compared with the classical nucleation theory. Figure 12 presents a comparison of the experimentally obtained nucleation rates with the CNT. The advantage of this kind of a plot is that the temperature dependence of experimental results is easier to interpret. It can be seen that the experimental results have a very similar temperature dependence. The ratio of the experimental and theoretical nucleation rates grows with increasing temperature. This means that the CNT cannot predict the temperature dependence of the measurements. The results of the new LFDC show a steepest trend as the results get closer to those measured by Lihavainen with increasing tempera-

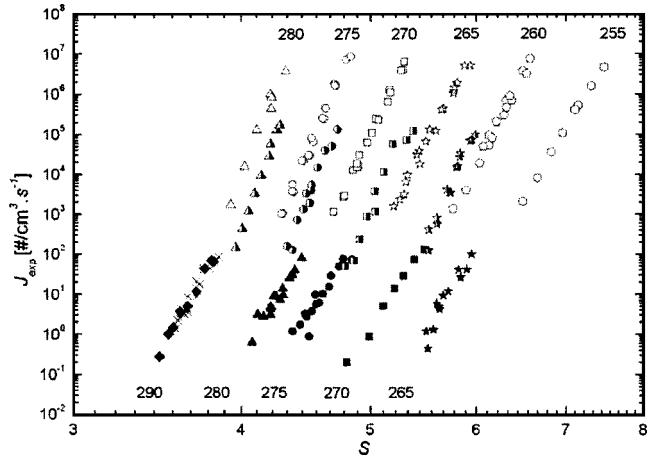

FIG. 9. The experimental nucleation rates J_{exp} as a function of saturation ratio S of 1-butanol. Filled symbols: TDCC at temperatures of 290, 280, 275, 270, and 265 K from left to right. Half-filled symbols: new LFDC at temperatures of 280, 275, 270, and 265 K from left to right. Open symbols: Lihavainen at temperatures of 280-255 K at 5-K intervals from left to right. Crosses: TDCC at temperature of 290 K and 120-kPa pressure.

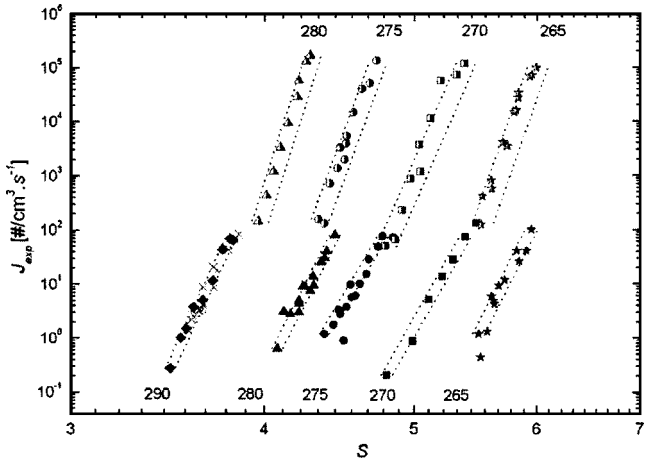

FIG. 10. The experimental nucleation rates J_{exp} as a function of saturation ratio S of 1-butanol. Filled symbols: TDCC at temperatures of 290, 280, 275, 270, and 265 K from left to right. Half-filled symbols: new LFDC at temperatures of 280, 275, 270, and 265 K from left to right. The dotted lines around the measured isotherms denote the estimated uncertainty.

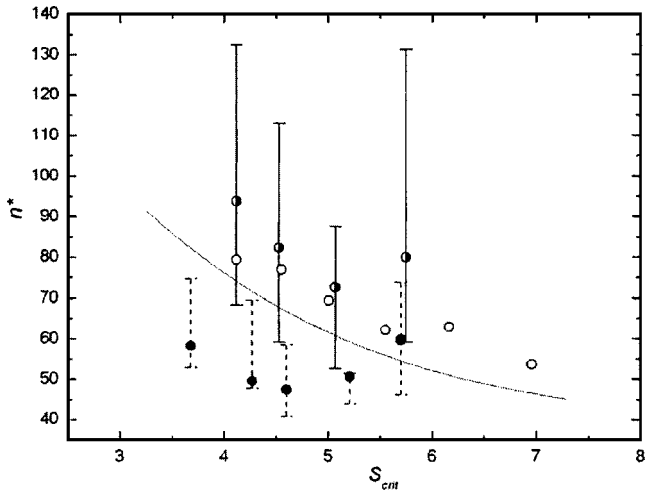

FIG. 11. Molecular content of the critical cluster $n^\star$ of 1-butanol as a function of critical saturation ratio S_{crit} taken from the middle of each isothermal measurement. The filled symbols: TDCC. The half-filled symbols: new LFDC. The open symbols: Lihavainen. The solid and the dashed error bars, respectively, represent the estimated uncertainty stemming from the uncertainties of the temperature measurements in the TDCC and the LFDC, respectively. The solid line denotes the prediction of $n^\star$ by CNT.

ture. The CNT underestimates the nucleation rates of both LFDCs but slightly overestimates those measured in the TDCC.

D. Comparison with other measurements

The kinetics of homogeneous nucleation of 1-butanol vapor has already been studied by Strey *et al.*[33] and Viisanen and Strey.[34] Both experiments were conducted in an expansion cloud chamber with argon as a carrier gas. The nucleation rate range in these measurements was about 10^5–10^9 cm^{-3} s^{-1}. The highest nucleation rates of the expansion chamber measurements and the lowest nucleation rates of the TDCC differ by nine orders of magnitude. Also the saturation ratios for the same isotherms are not the same, which complicate the qualitative comparison of results. It is largely accepted that the classical nucleation theory gives the correct saturation ratio dependency for isothermal measurements. With this in mind, the best way to compare the different measurements is to present them as a ratio between the experimental nucleation rates and those predicted by the CNT. This is done in Fig. 12. The nucleation rates measured by Viisanen and Strey overlap with those measured by Lihavainen and also have a similar temperature dependency. The measurements by Strey *et al.* have a different temperature dependency, J_{exp}/J_{the} decreases strongly as a function of increasing temperature. It should be noted that the data of Strey *et al.*[33] are not strictly isothermal. The results are close to those by Lihavainen at about 250 K, close to those measured in the new LFDC at about 270 K, and close to those measured in the TDCC at about 290 K. However, it is clear that this is merely coincidental. It should be noted that the validity of comparing the results from different measuring devices in this way depends on how well the theory predicts the saturation ratio dependency. For example, for the TDCC the nucleation rates depend less strongly on the saturation ratio. If a simple extrapolation was made to higher saturation ratios matching those of the expansion chamber measurements, the results would travel further away from each other.

V. ERROR ANALYSIS

The lowest measurable temperature in the new LFDC is limited by the evaporation of droplets during passage of the liquid drainage. The liquid drainage is not under temperature

TABLE IV. The difference, $\Delta n^\star$, between the critical cluster sizes from the nucleation theorem [Eq. (6)] and the Kelvin equation (7). S_{crit} is critical saturation ratio, T_n is nucleating temperature, and n^* number of molecules in critical cluster. The standard deviation(SD) is the statistical error obtained from isothermal plots.

S_{crit}, TDCC	T_n	n^*	SD	n^*(Kelvin)	Δn^*
3.68	290.0	58.3	0.1	80.8	−22.5
4.27	280.0	49.5	0.1	70.3	−20.7
4.60	275.0	47.4	0.2	66.4	−18.9
5.21	270.0	50.6	0.1	57.6	−6.9
5.70	265.0	59.8	0.2	53.9	5.9
S_{crit}, LFDC	T_n	n^*	SD	n^*(Kelvin)	Δn^*
4.12	280.0	93.8	0.1	75.7	18.1
4.53	275.0	82.3	0.2	68.4	13.9
5.07	270.0	72.7	0.3	60.5	12.2
5.75	265.0	80.0	0.2	53.1	26.9
S_{crit}, Lihavainen	T_n	n^*	SD	n^*(Kelvin)	Δn^*
4.12	280.0	79.4	0.2	75.8	3.6
4.55	274.9	77.0	0.1	67.8	9.2
5.01	270.0	69.4	0.1	61.9	7.5
5.55	264.9	62.2	0.1	56.5	5.7
6.16	260.0	62.9	0.1	51.9	11.0
6.96	254.9	53.7	0.1	47.1	6.6

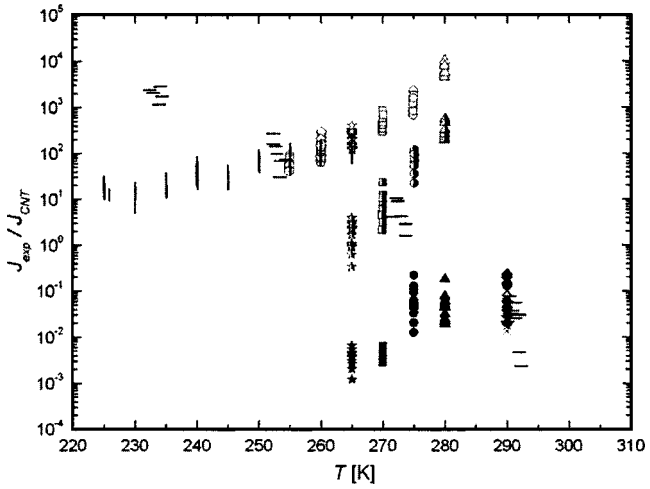

FIG. 12. The ratios of experimental nucleation rates J_{exp} and those predicted by the CNT as a function of temperature T. The filled symbols: TDCC. The half-filled symbols: new LFDC. The open symbols: Lihavainen. The vertical bars: Viisanen and Strey. The horizontal bars: Strey *et al.*

control and could only be cooled using ice if lower isotherms were measured. The error due to evaporation is more pronounced at low nucleation rates, making the slope of the isotherm steeper. This can especially be observed for critical cluster sizes (Fig. 11), where the n^* from the 265-K isotherm is higher than expected. To see the effect of evaporation, the slope of the 265-K isotherm with the new LFDC was also calculated from nucleation rates higher than 10^4 cm^{-3} s^{-1}. This resulted in critical cluster size around 50 molecules, which fits well into Fig. 11.

The purity of the carrier gas in the TDCC and the new LFDC was lower than that used by Lihavainen. This is not expected to influence the results.

VI. CONCLUSIONS

This work has introduced a new measurement, comparing devices based on the same principle, nonisothermal diffusion of the studied substance in the carrier gas. The thermal diffusion cloud chamber and two laminar flow diffusion chambers have been used to measure nucleation rates in the 1-butanol-helium system from cca 10^{-1}–10^2 cm^{-3} s^{-1} and 10^2–10^5 cm^{-3} s^{-1}.

The same isotherms were found at low saturation ratios with the LFDC and TDCC. The nucleation rates measured in the LFDC and the TDCC show a similar temperature dependence. Critical cluster sizes were obtained using the nucleation theorem. Both LFDCs provided very similar sizes slightly above the Kelvin equation, the TDCC suggests critical cluster sizes significantly smaller. It should be kept in mind that the range of nucleation rates and therefore the rate, at which the slope was determined, were different for both types of the chamber.

It was demonstrated, to what extent it is possible to change the slopes of measured isotherms by implementing unlikely large temperature uncertainty into the nucleation rate calculations. The space where the isotherms can be found with the highest probability is narrower concerning TDCC than LFDC. The same temperature error implemented into critical cluster size calculations generates an even more pronounced effect. If we take into account that the slopes were taken from opposite corners of the areas delimited by the dotted error lines, these deflections are again rather improbable extremes.

The differences in the results obtained by the two LFDCs are expected to arise from the different counting systems used for the determination of droplet concentration, since the errors in temperature measurements could not alone explain the differences, and the designs of the two LFDCs were otherwise deemed identical. Also the evaporation of droplets prior to counting was estimated to be higher in the recently built LFDC, because the liquid drainage in the LFDC of Lihavainen could be cooled below the condenser temperature.

The obtained results and overall behavior of all three devices correspond to previous measurements where similar substances were used. A comparison and subsequent deep analysis of the two devices (TDCC and recently built LFDC) were made in one laboratory by the same persons. This lowers the probability that the observed difference between the results is caused by any gross error.

Even though the three-order difference between TDCC and LFDC in the experimental nucleation rates looks large, it is, in fact, rather hidden in the uncertainties of the determination of the nucleation temperature and nucleation saturation ratio which are obtained as a solution of the model of coupled heat, mass and momentum transport.

Concerning the TDCC itself, it has been already shown elsewhere[35] that even if we replace the traditional 1D model, widely used in the case of TDCC, by a more rigorous two-dimensional (2D) model, the overall shift of the isotherm along the experimental nucleation rate coordinate is substantially less than one order of magnitude.

It is not clear, however, whether some improvement of the model describing transport processes in the LFDC would be able to explain the observed differences between the chambers.

ACKNOWLEDGMENTS

Support of this work by the Grant Agency of the Academy of Science of the Czech Republic (Grant No. IAA2076203) and by the Ministry of Education, Youth and Sports of the Czech Republic (Grant No. ME699) is gratefully acknowledged. This work was also supported by the bilateral exchange program between the Academy of Finland and the Academy of the Czech Republic. Two of the authors (D.B.) and (V.Ž.) would also like to thank the head of the Aerosol Laboratory, Dr. Jiří Smolík, for his long term support of nucleation research. The authors would also like to thank Dr. Hermann Uchtmann for providing the optical counting system for the LFDC.

[1] D. Kashchiev, J. Chem. Phys. **76**, 5098 (1982).
[2] M. P. Anisimov and A. G. Cherevko, Izv. Akad. Nauk. SSR, Ser. Khi. **2**, 15 (1983).
[3] R. C. Miller, R. J. Anderson, and J. L. Kassner, Jr., *Colloid and Interface Science* (Academic, New York, 1976), Vol. II, pp. 1–21.
[4] J. L. Schmitt, G. W. Adams, and R. A. Zalabsky, J. Chem. Phys. **77**, 2089 (1982).

[5]P. E. Wagner and R. Strey, J. Phys. Chem. **85**, 2694 (1981).
[6]R. Strey, P. E. Wagner, and Y. Viisanen, J. Phys. Chem. **98**, 7748 (1994).
[7]F. Peters, J. Chem. Phys. **77**, 4788 (1982).
[8]K. N. H. Loojimans, P. C. Kreisels, and M. E. H. van Dongen, J. Chem. Phys. **106**, 4152 (1993).
[9]Y. J. Kim, B. E. Wyslouzil, G. Wilemski, J. Wölk, and R. Strey, J. Phys. Chem. A **108**, 4365 (2004).
[10]J. L. Katz and B. J. Ostermier, J. Chem. Phys. **47**, 478 (1976).
[11]R. H. Heist and H. Reiss, J. Chem. Phys. **59**, 665 (1973).
[12]J. Smolík and J. Vítovec, Collect. Czech. Chem. Commun. **41**, 1471 (1976).
[13]C. Becker, H. Reiss, and R. H. Heist, J. Chem. Phys. **68**, 3585 (1978).
[14]C. Flageollet-Daniel, P. Erhard, and P. Mirabel, J. Chem. Phys. **75**, 4615 (1981).
[15]G. S. Cha, H. Uchtmann, J. A. Fisk, and J. L. Katz, J. Chem. Phys. **101**, 459 (1994).
[16]M. P. Anisimov and A. Cherevko, J. Aerosol Sci. **16**, 97 (1985).
[17]K. Hämeri and M. Kulmala, J. Chem. Phys. **105**, 7696 (1996).
[18]V. Vohra and R. H. Heist, J. Chem. Phys. **104**, 382 (1996).
[19]V. B. Mikheev, N. S. Laulainen, S. E. Barlow, M. Knott, and I. J. Ford, J. Chem. Phys. **113**, 3704 (2000).
[20]J. Smolík and P. E. Wagner, *Nucleation and Atmospheric Aerosols 1996, 14th International Conference on Nucleation and Atmospheric Aerosols*, Helsinki, 26–30 August 1996, edited by M. Kulmala and P. E. Wagner (Pergamon, New York, 1996), pp. 58–60.
[21]H. Lihavainen and Y. Viisanen, J. Phys. Chem. B **105**, 11619 (2001).
[22]H. Lihavainen, Ph.D. thesis, Finnish Meteorological Institute, 2000; Report Series in Aerosol Science No. 45, ISSN 0784-3496 (Finnish Association for Aerosol Research, Helsinki, 2000).
[23]V. Ždímal and J. Smolík, Atmos. Res. **46**, 391 (1998).
[24]M. P. Anisimov, V. G. Kostrovskii, and M. S. Shtein, Kolloidn. Zh. **40**, 90 (1978).
[25]J. Smolík and V. Ždímal, Aerosol Sci. Technol. **20**, 127 (1994).
[26]V. Ždímal, J. Smolík, P. K. Hopke, and J. Matas, *Book of Abstracts, 15th International Conference Nucleation and Atmospheric Aerosols 2000*, Rolla, USA, 6–11 August 2000, edited by B. Hale and M. Kulmala (American Institute of Physics, New York), pp. 311–314.
[27]J. Smolík and J. Vašáková, Aerosol Sci. Technol. **14**, 406 (1991).
[28]P. E. Wagner and M. P. Anisimov, J. Aerosol Sci. **24**, 103 (1993).
[29]M. P. Anisimov, K. Hämeri, and M. Kulmala, J. Aerosol Sci. **1**, 23 (1994).
[30]R. Becker and W. Döring, Ann. Phys. **26**, 719 (1935).
[31]A. Bertelsmann and R. H. Heist, J. Chem. Phys. **106**, 610 (1997).
[32]A. Bertelsmann and R. H. Heist, J. Chem. Phys. **106**, 624 (1997).
[33]R. Strey, P. E. Wagner, and T. Schmeling, J. Phys. Chem. **84**, 2325 (1986).
[34]Y. Viisanen and R. Strey, J. Chem. Phys. **101**, 7835 (1994).
[35]F. Stratmann, M. Wilck, V. Ždímal, and J. Smolík, J. Phys. Chem. B **105**, 11641 (2001).
[36]B. E. Poling, J. M. Prausnitz, J. P. O'Connell, *The Properties of Gases and Liquids*, 5th ed. (McGraw-Hill, Singapore, 2000).
[37]R. C. Reid, J. M. Prausnitz, and B. E. Poling, *The Properties of Gases and Liquids*, 4th edition (McGraw-Hill, New York, 1987).
[38]C. L. Yaws, Chem. Eng. (Rugby, U.K.) **22**, 153 (1976).
[39]R. Strey and T. Schmeling, Ber. Bunsenges. Phys. Chem. **87**, 324 (1983).
[40]T. Schmeling and R. Strey, Ber. Bunsenges. Phys. Chem. **87**, 871 (1983).
[41]C. H. Hung, M. J. Krasnopoler, and J. L. Katz, J. Chem. Phys. **90**, 1856 (1989).
[42]J. Vašáková and J. Smolík, Rep. Ser. Aerosol Sci. **25**, 1 (1994).